Synaptically induced changes in cell volume in the rat hippocampal slice

Sachiko Takagi

Department of Physiological Sciences, School of Life Science,

The Graduate University for Advanced Studies

Contents

Summary

Swelling of brain cells is one of the physiological responses associated with neuronal activation. To investigate underlying mechanisms, we analyzed interactions between changes in cell volume and synaptic activities in the hippocampal slices from rodents. Electrical stimulation was delivered through a bipolar electrode placed on the stratum radiatum or the stratum oriens/alveus. Swelling within the CA1 area were detected as increases in transmittance of near-infrared light (IR), and field excitatory postsynaptic potentials (fEPSPs) were recorded simultaneously. High frequency stimulation (HFS) of afferent fibers induced a transient increase in IR transmittance in both somatic and dendritic regions, which was temporally associated with the summation of fEPSPs. Stimulus-induced increases in transmittance were strongly reduced in the presence of APV and CNQX, indicating involvement of glutamate receptors. Application of a GABA-A receptor antagonist, bicuculline, increased the amplitude and time course of the fEPSPs but rather decreased HFS-induced optical signals. When the extracellular Cl^- was reduced to 10.5 mM, HFS induced a decrease in transmittance, which was also blocked by bicuculline. In hippocampal slices obtained from mice deficient in the 65 kDa isoform of glutamic acid decarboxylase, HFS-induced signals were significantly smaller than in the wild-type mice, although fEPSP profiles did not differ. These results suggest that both activation of glutamate receptors and Cl^- influx through GABA-A receptors contributes to synaptically evoked swelling in the hippocampal CA1 region.

Introduction

Regulation of cell volume is an essential function of most mammalian cells (Strange et al., 1996; Okada et al. 2001). In the cells of the central nervous system, maintenance of cell volume is particularly crucial because of the restrictive nature of the skull. In neurons, in addition to osmotic regulation of cell volume, physiological swelling occurs as a result of membrane depolarization and subsequent firing (Andrew and MacVicar, 1994; Schwartzkroin et al., 1998). Under the condition where excessive and synchronous electrical discharges occur such as epilepsy, it is particularly important for individual neurons to maintain the ability to restore cell volume, because prolonged depolarization due to recurring seizures could induce pathological swelling, leading to cell death (Andrew et al., 1989; Jefferys, 1995; Turner et al., 1995; Dudek et al., 1998). Mass changes in volume of cortical cells in response to electrical stimulation can be detected in terms of characteristics of extracellular spaces *in vivo* (Dietzel et al., 1980; Prichard et al., 1995; Anderson et al., 1996; Zhong et al., 1997; Nicholson and Sykova, 1998). In the human brain, transient swelling of cortical cells due to visual stimulation was recently detected by diffusion-weight magnetic resonance imaging (DW-MRI) (Darquie et al., 2001). While neuron excitation causes changes of cell volume, conversely, cell swelling enhances neuronal responses. The narrowed extracellular space accelerates excitation of local neuron population. A hypo-osmotic environment induces epileptic discharges of neurons, whereas such activity is inhibited under hyper-osmotic conditions (Dudek et al., 1990; Ballyk et al., 1991). Excitatory postsynaptic potentials (EPSPs) are enhanced during hypotonic challenge of neocortical neurons (Rosen and Andrew, 1990). In CA1 region of hippocampal slices, extracellularly recorded field EPSPs (fEPSPs)

increase but intracellular EPSPs do not (Ballyk et al., 1991). The enhanced excitability caused by extracellular hypotonia has been attributed to the increased ephaptic interaction among swollen neurons, caused by the obliteration of interstitial spaces (Dudek et al., 1990; Ballyk et al., 1991). These evidences suggest existence of mutual relationships between neuronal activity and the cell volume.

Cell volume regulation involves a variety of pathways, with considerable differences between cell types. One common pathway activated during hypo-osmotic stress involves Cl^- channels. However, hypo-osmotically stimulated anion permeability can be regulated by a diverse array of second messengers (Basavappa and Ellory, 1996). Although neuronal swelling can occur in a number of pathological and nonpathological conditions, our understanding of neuronal volume regulation is limited. Mechanisms underlying activity-dependent volume changes have been pursued in several *in vitro* studies using brain slice preparations. Some studies have suggested that strong excitation of neurons induces K^+ efflux into the extracellular space, which results in swelling of neighboring glial cells by activation of different transporters (MacVicar and Hochman, 1991; Murase et al., 1998; Holthoff and Witte, 2000; MacVicar et al., 2002), the authors concluding that the contribution of neurons to tissue swelling might be minor. However, other groups demonstrated that application of glutamate agonists could induce neuronal swelling in slices (Andrew et al., 1996; Jarvis et al., 1999) and in single cell preparations (Inglefield and Schwartz-Broom, 1998). However, mechanisms and candidate ion channels and/or transporters which might be involved remain unclear.

In the present study, hippocampal slices obtained from rodents were imaged for transmittance of near infrared light, to investigate mechanisms of activity-dependent swelling of brain cells. It has been difficult to measure the dynamic nature of cell swelling

and cell volume recovery in real time. In brain slices cell swelling has not been measured directly but has been inferred from decreases in overall light reflectance (Lipton, 1973), from increases in extracellular tissue resistance (Traynelis and Dingledine, 1989) or from reductions in extracellular space as measured by diffusable, impermeable markers (McBain et al., 1990; Nicholson, 1992). These techniques are accurate but their spatial resolution has been limited. On the other hand, the measurement of intrinsic optical signals by CCD-generated images permits the monitoring of extensive regions of brain tissue in real time. Light transmittance is a form of intrinsic optical signaling known to directly correlate with neuronal synaptic depolarization and activity-induced swelling (Andrew and MacVicar, 1994; Kreisman et al., 1995; Holthoff and Witte, 1996; Isokawa and Mathern, 1999). In hippocampal slices, blocking synaptic transmission with either Ca^{2+}-free perfusate or kynurenic acid (an excitatory amino acid antagonist) abolished the optical signals (MacVicar and Hochman, 1991). In the present study, we successfully detected synaptically induced swelling in the CA1 regions, and found that Cl^- influx through GABA-A receptors has a significant role.

Materials and Methods

Hippocampal slice preparation

All experiments were performed according to the guidelines of the animal welfare committee of the National Institute for Physiological Sciences. Two- to 3-week-old Sprague Dawley rats or 15-week-old outbreed C57BL6 x 129SV (GAD65(+/+), GAD65(−/−)) mice were deeply anesthetized with ether and decapitated. The brains were quickly removed and hemisected on a filter paper moistened with a cutting solution of the following composition (in mM): 120 choline-Cl, 3 KCl, 8 $MgCl_2$, 1.25 NaH_2PO_4, 26 $NaHCO_3$, and 20 glucose, equilibrated with 95% O_2- 5% CO_2. Brain tissues containing the hippocampi on both sides were dissected out and placed in a cutting chamber filled with ice-cold cutting solution. Blocks were sliced into 400 μm sections transversely to their longitudinal axis using a vibrating microtome (Campden Instruments, Lafayette, IN), followed immediately by incubation at room temperature for 1 hour and a half in a reservoir chamber filled with normal solution. The normal recording solution was composed of (in mM) 125 NaCl, 2.5 KCl, 2 $CaCl_2$, 2 $MgCl_2$, 1.25 NaH_2PO_4, 26 $NaHCO_3$, and 10 glucose (334 mOsm), bubbled with a mixture of 95% O_2- 5% CO_2, making the final pH 7.4. For low-Cl^- solution, 125 mM NaCl was replaced with the same concentration of Na-isethionate. To test the effects of osmotic perturbations, modified standard solutions composed of (in mM) 65 NaCl, 2.5 KCl, 2 $CaCl_2$, 2 $MgCl_2$, 1.25 NaH_2PO_4, 26 $NaHCO_3$, 10 glucose and 0-180 mannitol (223-390 mOsm) were also prepared.

Electrophysiological recordings

A single slice was transferred to submerged chamber mounted on the stage of an upright microscope (BX50WI, Olympus Optical, Tokyo, Japan), and superfused continuously (1 ml/min) with normal solution. Temperature of the solution was regulated at 35 ± 1°C. For electrical stimulation of the afferent inputs or the efferent fibers, bipolar stimulation electrodes constructed from thin tungsten wire (50 μm OD) were placed on the stratum radiatum or the stratum oriens/alveus in the CA1-2 region. Duration and intensities of stimulation pulses were 100 μsec and 2-80 μA, respectively. Single or a train of pulses (1-100 pulses/sec, 10-200 pulses) was delivered. Field excitatory postsynaptic potentials (fEPSPs) were recorded with a glass electrode (1.5 mm OD, thick-walled glass tubing (1511-M, Friedrich & Dimmock, Melville, NJ) from the stratum radiatum or the stratum pyramidale of the CA1 region. The electrode was filled with 2 M NaCl. In some experiments, intracellular recordings were made of CA1 pyramidal neurons using patch pipettes pulled from the same type of glass tubing. The pipette solution contained (in mM) 130 K-gluconate, 10 NaCl, 10 N-2-hydroxyethylpiperazine-N'-2-ethanesulfonic acid (HEPES), 4 $MgCl_2$, pH adjusted to 7.3 with KOH. Open resistance of the pipettes was 5-7 MΩ.

Imaging of intrinsic optical signals

Slices were trans-illuminated by near-infrared light (775 ± 15 nm, band-pass) from a halogen lamp whose power was regulated to minimize fluctuation (< 0.1%). Images of transmittance were obtained using a 12-bit cooled CCD camera system (Merlin, Life Sciences Resources, Hialeah, FL) at 125 ms per a frame. A schematic drawing of the experimental setup is given in figure 1. Activity-dependent changes in light transmittance of selected regions were presented as the spatial average of ΔT/T (percent), where T is the

transmittance intensity and ΔT/T is the time-dependent change in transmittance. Each record was smoothed by a 13 point moving average to reduce noise.

Ten micro M 6-cyano-7-nitroquinoxaline-2,3-dione (CNQX) and 50 μM DL-2-amino-5-phosphonovaleric acid (APV) were added to the perfusing solution to eliminate fast glutamatergic input, and 20 μM bicuculline methiodide (BMI), 10 μM SR95531 or 10 μM picrotoxin was added to block GABAergic input. Bumetanide, furosemide, dihydroindenyloxyalkanoic acid (DIOA), 4,4'-diisothiocyanatostilbene-2,2'-disulfonic acid (DIDS), 5-nitro-2-(3-phenylpropylamino-benzoate) (NPPB), r-[+]-methylindazone (IAA-94) or glibenclamide was applied to the perfusing solution to estimate contribution of transporters and other Cl^- pathways.

Morphological analysis in single neuron by using two-photon laser microscopy

Slices were incubated at 35 ± 1°C for 1 hour in a reservoir chamber filled with normal solution containing 5 μM calcein-AM (Molecular Probes, Inc.). A single slice was transferred to submerged chamber mounted on the stage of an inverted microscope (IX70, Olympus Optical, Tokyo, Japan), and superfused continuously (1 ml/min) with normal solution containing 1 mM tetraethylammonium (TEA) and 100 μM 4-aminopyridine (4-AP) regulated at 35 ± 1°C. A two-photon scanning unit (MRC1024MP, Bio-Rad, Inc.), a mode-locked titanium-sapphire laser (Tsunami, Spectra Physics, Mountain View, California) and a photo-diode pump laser (Millennium, Spectra Physics) were attached to the microscope. For stimulation, bipolar stimulation electrodes constructed from thin tungsten wire (50 μm OD) were placed on the stratum radiatum in the CA1-2 region. Consecutive image sections of a stained pyramidal neuron in CA1 area were captured in

each focus (distance between sections, 0.4 μm) at time periods before, just after and 5 min after stimulation. Cell boundaries were detected by applying an edge detection scheme to each 2-dimension (2D) image (Photoshop, Adobe). Three-dimensional reconstruction from the 2D images was carried out using TRI 3D-Viewer software (Ratok systems, Inc.).

SR95531 was purchased from Tocris Cookson (Bristol, UK). APV, CNQX and all other compounds were obtained from Sigma/RBI Chemical (St. Louis, MO).

Results

Reliability of the imaging system

Increases in the cell volume were detected as an increase in light transmittance. In the beginning of a series of experiments, we analyzed optical signals obtained from hippocampal slice in response to hypo- and/or hyper-osmotic stress, to estimate reliability and accuracy of our imaging system. Time dependent changes in light transmittance in several hypo-osmotic conditions were shown in figure 2A. When osmolality of perfusing solution was reduced, optical signal start to increase with a short delay, and made peaks. Increases in transmittance were quickly returned and made 'undershoot' when perfusing solution was replaced with normal-osmotic solution. The signal completely recovered to original level within 60 min. These patterns of the optical signal were very similar to the pattern of relative change in volume of single cell in response to hypotonic conditions. Peak changes in light transmittance as a function of bath osmolarity were shown in figure 2B. At least in the range from 223 to 390 mOsm, changes in light transmittance and extracellular osmolarity showed linear relationship. In human epithelial cells, it is reported that relationship between bath osmolarity and relative cell volume follows the van't Hoff's theory, and it can be represent as following equation (Morishima et al., 2000): $V/V_0=0.75(\pi_0/\pi)+0.25$, where V is volume of the cell in the test bath solution, V_0 is volume of the cell in the control bath solution, π is osmolarity of the test bath solution, π_0 is osmolarity of the control bath solution. According to this theory, therefore, it is possible to speculate relationship between changes in light transmittance and average changes in volume of cells in a slice (fig 2C). Plots were well fitted by linear regression ($r = 0.997$, slope = 0.0081). Taken together, we conclude that our imaging system would be

useful to detect changes in cell volume induced not only by changes in bath osmolarity but also by neuronal activations.

Changes in IR transmittance induced by electrical stimulation in hippocampal slice

Procedures of main experiments and an example of near-infrared (IR) images are illustrated in figure 3A. By using our imaging system, increases in the cell volume were detected as an increase in light transmittance. Neuronal activities, including synaptic responses, were simultaneously recorded from the stratum radiatum of CA1 region. When high frequency stimulation (HFS) was delivered to afferent fibers, transient increases in IR transmittance in both somatic and dendritic regions were observed. Figure 3B shows typical traces of extracellular recordings and changes in the transmittance in response to HFS (100 pulses/sec, 20 pulses). The increase in IR transmittance recovered gradually to control levels within 80-100 sec. Interval of each optical recording was longer than 5 min. To examine the contribution of action potentials to the optical signals, a train of antidromic stimulation was delivered to efferent fibers in the presence of glutamate receptor antagonists. Intracellular recordings from pyramidal neurons confirmed generation of a somatic spike train. However, antidromic stimulation did not induce changes in transmittance in any region (data not shown), indicating that synaptic input is required for the increase in cell volume.

Participation of neuronal swelling in the optical signal

Increase in light transmittance represents swelling of cells. However, it did not directly indicate swelling of neurons. To confirm that neuronal swelling participate in increase in light transmittance, we performed following three preliminary experiments.

First, we morphologically examined whether pyramidal neuron swell by electrical stimulation, by using two-photon laser scanning microscopy. Experimental procedure was shown in figure 4A. Three-dimensional images of pyramidal neurons were reconstructed from consecutive section image at each period before, just after and 5 min after electrical stimulation (see methods). One mM TEA and 100 μM 4-AP were always existed in bath solution because some of convulsant drugs, such as TEA or 4-AP, are reported to enhance changes in light transmittance in response to electrical stimulation (see D'Arcangelo et al., 2001). We measured cross-sectional area of midline section of somato-dendritic axis in each reconstructed image of cell. Figure 4B shows section areas at each distance from head of the soma in the three periods mentioned above. After repetitive stimulation (2 pulses/sec, 20 pulses), clear increases in section area were seen in the soma and the proximal dendrite, and these were completely recovered at 5 min after stimulation. Normalized changes in section areas obtained from 6 neurons were summarized in figure 4C. Because of variety in somatic size, we adjusted distances at a section showing maximum section area as a landmark (distance 0). Section areas significantly increased after stimulation at the region from the soma to the proximal apical dendrite, and recovered within 5min. These results clearly indicate that neuron swells by electrical stimulation.

Second, we imaged light transmittance with slices treated with gliotoxin, fluorocitrate, for 6 hrs. It is reported that 2 hrs treatment with fluorocitrate resulted in damage of astrocytes (Paulsen et al., 1987; Yoshioka et al., 2000). Therefore, glial cells in our treated slice should be more heavily damaged, and increases in light transmittance might be reduced if the optical signal was originated from glial cells. However, stimulus-induced increases in transmittance were similarly observed in the CA1 region

and the peak signals were comparable with these obtained from non-treated slices (data not shown). Therefore, contribution of the optical signal from glial cells would be negligible.

Furthermore, we imaged stimulus induced optical signal with slices from gerbils 7 days after transient ischemia. Since all pyramidal neurons in the CA1 region are known to be lost and filled with glial cells at 7 days after forebrain ischemia (Kirino, 1982; Pulsinelli et al., 1982), increases in light transmittance might be reduced if the optical signal was mainly originated from neurons. Stimulus-induced increases in transmittance were almost abolished in the CA1 region, but small peaks (less than 0.5%) were still observed (data not shown). This week signal was remained when extracellular Ca^{2+} was replaced with Mg^{2+}, but completely inhibited by TTX application. Therefore it could be originated from axon arbors probably coming from CA2-3 neurons.

From results obtained from above preliminary experiments, we conclude that, at least in our imaging system, activity-dependent increase in transmittance in the CA1 region mainly reflects swelling of neurons.

Basic properties of the optical signals

Under our recording conditions at slice experiments, peak changes in the transmittance were positively correlated with the stimulus frequency and the number of stimulation pulses (fig. 5A, B). Since there were no significant differences between somatic peaks and dendritic peaks at each stimulus condition, changes in the signals from both regions as a function of stimulus parameters could be basically identical. Peak changes also increased with stimulus intensities from 2 to 20 μA (fig. 5C). Although the amplitude of population spikes in the somatic field potentials increased with the stimulus

intensity from 20 to 80 μA, the peak signals did not significantly vary, indicating that generation of somatic spikes is not necessary for the swelling (fig. 5C). We used stimulus intensities higher than 20 μA for further experiments.

Contribution of glutamatergic excitatory input to the swelling

Stimulus-induced increases in transmittance were strongly reduced in the presence of glutamate receptor antagonists. Figure 6 shows effects of bath application of 50 μM APV and 10 μM CNQX. Field potentials recorded from the stratum radiatum were completely abolished in the presence of these drugs. The optical signals induced by HFS (100 pulses/sec, 20 pulses) were reduced, and recovered by washing out the drugs (fig. 6B). Effects on the peak optical signals obtained from somatic and dendritic regions are summarized in figure 6C. There were significant differences between peak responses in controls (mean ± SD, 2.0 ± 0.7% for the stratum radiatum, 1.8 ± 0.7% for the stratum pyramidale, n = 40) and in the presence of APV and CNQX (0.5 ± 0.1% for the stratum radiatum, 0.4 ± 0.1% for the stratum pyramidale, n = 9) ($P < 0.01$), indicating that activation of NMDA and/or AMPA receptors is required for induction of activity-dependent swelling. In the presence of APV and CNQX, there remained some fraction of the optical signals although the fEPSPs were completely eliminated. Since this 0.5% fraction also detected in Ca^{2+}-free perfusate, and completely abolished by application of 1 μM TTX (data not shown), it is suggested that this remained fraction reflects swelling of axons and/or glial cells.

Contribution of GABAergic inhibitory input to the swelling

The contribution of GABAergic input to the optical signals was also investigated.

Figure 7 demonstrates a typical effect of bicuculline on field potential and optical signals. Since bicuculline (20 μM) reversibly increased the amplitude and time course of the field potential (fig. 7A), we expected that stimulus-induced optical signals might also be enhanced. However, HFS-induced optical signals were rather reduced in the presence of the GABA-A receptor antagonist. When 20 μM bicuculline was applied to the perfusing solution, increases in the transmittance in response to tetanic stimulation (100 pulses/sec, 20 pulses) were significantly inhibited in both somatic and dendritic regions (fig. 7B). Bicuculline did not change baseline transmittance. Inhibition of optical signals was moderate compared with the effect of blockade of glutamate receptor channels, but there was a significant difference between control responses and those in the presence of bicuculline ($1.0 \pm 0.4\%$ for the stratum radiatum, $0.9 \pm 0.4\%$ for the stratum pyramidale, $n = 17$) ($P < 0.01$) (fig. 7C). Similar results were obtained when we used another GABA-A receptor antagonist, SR95531 (10 μM), or picrotoxin (10 μM) (data not shown). Moreover, application of 50 μM APV and 10 μM CNQX in addition to 20 μM bicuculline, the optical signals induced by HFS were further reduced ($0.5 \pm 0.1\%$ for the stratum radiatum) (data not shown). To examine the role of Cl^- influx through GABA-A receptor channels, we measured HFS-induced signals when the extracellular solution was stepwise depleted of Cl^- (72.5 mM, 41.5 mM, 10.5 mM) (fig. 8A). The peak amplitude of HFS-induced signals was decreased according to the extracellular Cl^- concentration ($n = 6$). At 10.5 mM, HFS-induced optical signals were reversed, suggesting that the cell volume was rather decreased. In this case, usually recovery took longer time (120-180 sec) probably because recovery of cell volume from shrinkage depends on different mechanisms. We could not characterize an early increasing component. However, since it was insensitive to glutamate receptor and GABA-A receptor antagonists, it might be

originated from fibers and/or glial cells. In all slices that it was tested (n = 5), HFS-induced decreases in the transmittance were also blocked by application of bicuculline (fig. 8B), indicating that activation of GABA-A receptors is involved in induction of stimulus-induced swelling and suggesting that Cl^- influx through GABA-A channels at synapses is a major cause of swelling in the CA1 region.

To examine whether GABA released from inhibitory presynaptic terminals contributes to the activity-dependent swelling, we used hippocampal slices prepared from mice deficient in the 65 kDa isoform of glutamic acid decarboxylase (GAD65(−/−)). Tian (Tian et al., 1999) reported that both the quantal size and frequency of GABA-mediated spontaneous IPSCs appear to be normal in GAD65(−/−) mice, but that the release of GABA is reduced during sustained stimulation. Therefore, which is involved in GABA-synthetic pathways. It would be expected that this mutant mouse fails to release sufficient GABA when presynaptic terminals are strongly activated. Figure 6 shows typical results obtained with wild-type (GAD65(+/+)) and mutant (GAD65(−/−)) mice. There was no difference between the kinetics of field potentials in the two strains (fig. 9A), probably because the amount of GABA release in response to a single stimulation did not differ (see Tian et al., 1999). In the presence of bicuculline, amplitude and time course of fEPSPs were increased in both mice (data not shown). However, in mutant mice, HFS-induced increases in IR transmittance in the CA1 region were significantly smaller than those obtained in wild-type mice (fig. 9B). Peak changes in optical signals in wild-type and GAD65(−/−) mice were 2.0 ± 0.7% (n = 10) and 0.8 ± 0.5% (n = 14), respectively ($P < 0.01$) (fig. 9C). Moreover, the effects of a GABA-A receptor antagonist on the optical signal were negligible in the mutant mice, although significant decreases occurred in the wild-type (in control 2.0 ± 0.7%, in the presence of bicuculline 0.8 ±

0.3%, n = 10) ($P < 0.01$). Taken together, the results in the present study suggest that Cl^- influx into postsynaptic neurons through GABA-A receptor channels that are activated by synaptically-released GABA is a major cause of activity-dependent swelling in the hippocampal CA1 region. A possible mechanism underlying synaptically-induced swelling of the hippocampal pyramidal neuron was illustrated in figure 10.

Contribution of other pathways for Cl^- entry

Even in the presence of GABA-A receptor antagonists, there remained some component of optical signals. Therefore we performed pharmacological analyses to examine the possible contribution of other Cl^- pathways including the voltage-dependent Cl^- channel, the Ca^{2+}-activated Cl^- channel, the $Na^+/K^+/2Cl^-$ co-transporter and the volume-sensitive Cl^- channel (table 1). However, no positive effects were observed except with 100 μM dihydroindenyloxyalkanoic acid (DIOA), an inhibitor of K^+/Cl^- co-transporter and HCO_3^-/Cl^- exchanger (data not shown). DIOA perfusion may predominantly induce hyperpolarization of presynaptic fibers, which was caused by changes in local K^+ gradient following blockage of K^+/Cl^- co-transporter. Bath application of DIOA induced inhibition of fEPSPs in all slices tested. Since the effect on the optical signal (a decrease in the peak signal) might be caused by the reduction of fEPSPs, we did not use the data for further analysis. A high concentration of furosemide (2.5 mM) also effectively decreased the peak optical signal. However, we could not specify the target because of its poor selectivity. Further precise analysis is required to find origin of remaining component of the optical signals.

Discussion

Origin of intrinsic optical signals

Several functions of neurons in the brain have been investigated by using imaging of intrinsic optical signals (IOS) (Grinvald et al., 1986; Haglund et al., 1992; Shoham and Grinvald, 2001). The main origin of intrinsic signals in *in vivo* preparations is known to be a change in blood flow rate or the proportion of oxidized hemoglobin (Frostig et al., 1990). However, in slice preparations without blood flow, the dominant source of intrinsic signals is a change in light scattering, due to variation in tissue architecture such as caused by swelling (MacVicar and Hochman, 1991). Transmittance imaging is able to detect swelling of cells by a decrease in scattered particles in a unit volume of brain tissue (Momose-Sato et al., 1998; Jarvis et al., 1999; Johnson et al., 2000). When brain slices are perfused with hypo-osmotic solution, cells swell and light transmittance increases (Andrew and MacVicar, 1994; Kreisman et al., 1995). An alternative method is to estimate the volume of extracellular spaces by measuring the extracellular concentration of tetrametyl ammonium (TMA) using ion-selective electrodes (Nicholson and Sykova, 1998; Witte et al., 2001). Holthoff and Witte (1996) performed imaging of intrinsic signals and measured TMA concentrations simultaneously in slice preparations, and reported spatial and temporal matching. Therefore, the idea that increases in light transmittance reflect swelling of cells is now well established. We also checked calcein fluorescence in the extracellular space decreased when electrical stimulation was delivered.

In the present study, transient increases in transmittance were detected in both somatic and dendritic regions in response to repetitive synaptic inputs, but the time

course differed between the two cases. We found that the time to peak optical signals was always faster, and the amplitude of the peak was always larger in the stratum radiatum than in the stratum pyramidale. Although the region of IOS measurement is not strictly determined by boundaries of layers, these differences were probably due to variation in tissue components in the two regions. The pyramidal cell layer is filled with cell bodies and few neuronal processes, whereas the stratum radiatum is composed of dendrites and axons as well as glial cells and other connective tissues. It is therefore quite probable that these different structures would have their own patterns of swelling. Here we could only measure spatial averages for the combinations of such multiple components.

In the present study, using IOS imaging, we detected swelling in the hippocampal CA1 region induced by electrical stimulation of afferent fibers. Because of low magnification microscope optics, it is difficult to distinguish swelling of neurons from that of other structures including glial cells (Andrew et al., 1999). However, previous studies with fluorescence imaging of single neurons demonstrated that application of NMDA- and/or AMPA-receptor agonists induced swelling (Andrew et al., 1996; Inglefield and Schwartz-Bloom, 1998; Jarvis et al., 1999). Our results from two-photon experiments provided neuronal swelling induced by electrical stimulation. In our preliminary experiments with slices treated with gliotoxin, fluorocitrate, for 6 hrs, stimulus-induced increases in transmittance were similarly observed in the CA1 region. Since morphological study shows 2 hrs treatment with fluorocitrate resulted in damage of astrocytes (Paulsen et al., 1987; Yoshioka et al., 2000), glial cells in our treated slice should be more heavily damaged. Therefore, in the present experiments, it is supposed that activity-dependent swelling in the CA1 region mainly reflect swelling of neurons. Furthermore, in our preliminary other experiments with slices from gerbils 7 days after

transient ischemia, stimulus-induced increases in transmittance were observed in the CA1 region but the peaks were usually less than 0.5% and insensitive to glutamate receptor antagonists. Since all pyramidal neurons in the CA1 region are known to be lost and filled with glial cells at 7 days after forebrain ischemia (Kirino, 1982; Pulsinelli et al., 1982), the week signals could not have been due to neurons. Therefore, in the present experiments, activity-dependent swelling in the CA1 region required, at least, activation of glutamate receptors in neurons.

Mechanisms underlying HFS-induced swelling

Swelling of hippocampal CA1 regions was induced by electrical stimulation of afferent fibers, which make glutamatergic excitatory synapses and GABAergic inhibitory synapses on postsynaptic neurons. The contribution of Na^+-dependent action potentials must have been small because the peak amplitude of the transmittance was not significantly altered even when large population spikes were detected in field potentials. MacVicar and Hochman (1991) also reported that activation of grutamate receptors is required for induction of activity-dependent swelling. We confirmed their results about this point. Moreover, in their experiments, either application of 2.5 mM furosemide or reduction of extracellular Cl^- resulted in reduced signals. Since furosemide blocks $Na^+/K^+/2Cl^-$ co-transporters, which predominantly exist on glial membranes, they hypothesized that accumulation of extracellular K^+ by neuronal activation may induce glial swelling by ionic influx through the $Na^+/K^+/2Cl^-$ co-transporter and consequent water influx. Indeed, an increase in extracellular K^+ induces the increase in light transmittance in slices, and high-K^+ induced swelling is inhibited by bumetanide (MacVicar et al., 2002). In our present experiments, we tested this compound, a selective

antagonist for $Na^+/K^+/2Cl^-$ co-transporter, but no effects were evident on optical signals. While inhibition was noted with 2.5 mM furosemide, additional application of bicuculline was without influence. Recent reports (Evans et al., 1986; Pearce, 1993; Martin et al., 2001) indicate that a high concentration of furosemide can block other channels such as the Ca^{2+}-activated Cl^- channel and the GABA-A receptor channel. Therefore, the inhibition of optical signals by furosemide in our study could be due to its impact on GABA-A receptors. So that optical signals analyzed in our experiments may mainly reflect swelling of neurons. In our hypothesized model of swelling (fig.10), Na^+ and Ca^{2+} influxes through AMPA and NMDA receptors induce an increase in intracellular osmotic pressure, which facilitates water influx into the cell. As the counterpart to these cations, we propose that Cl^- is the main anion, and with activation of GABA-A receptors as the main process during the Cl^- influx. However, even in the presence of bicuculline, small but a clear transient signal remained in response to stimulation. Therefore, our results do not exclude a possible contribution of the other pathways for anion, such as K^+/Cl^- co-transporter and HCO_3^-/Cl^- exchanger.

In cortical slices, application of bicuculline enhances IOS induced by high frequency stimulation (HFS) of afferent fibers (Dodt et al., 1996; Kohn et al., 2000), whereas application of furosemide causes its reduction (Holthoff and Witte, 1996). Since this has been explained on the basis of signals originating from glial cells, the contribution of neuronal GABA-A receptors to swelling must be negligible. Enhancement of stimulus-induced IOS by bicuculline has also been reported with slice through hypothalamic regions (Trachsel et al., 1996). Further precise analysis is required to clarify whether different brain regions have their own mechanisms underlying swelling.

Physiological relevance

It has been suggested that a functional deficit in the brain inhibitory system is closely related to generation of temporal lobe epilepsy in the human brain (During and Spencer, 1993; Isokawa, 1996). Selective loss of GABAergic interneurons has recently been observed in the hippocampus in an experimental epilepsy model (Morin et al., 1999; Cossart et al., 2001). Interestingly, when AMPA is applied, hippocampal slices obtained from both the pilocarpine model of epilepsy and patients whose hippocampi are sclerotic show less swelling than control slices (Isokawa, 2000). Since the GAD65 KO mouse is prone to epileptic seizure as a behavioral phenotype (Asada et al., 1996), our results suggest that the GABAergic system is not only required for stabilizing neuronal activities but also significant for swelling in the hippocampal CA1 region. There have been several previous reports in the literature of a positive contribution of tissue swelling to epileptic neuronal activity (Andrew et al., 1989; Dudek et al., 1990; Ballyk et al., 1991; Jefferys, 1995; Dudek et al., 1998). It might be expected that generation, synchronization and/or propagation of epileptic activity may be caused by a variety of different mechanisms (see Hochman et al., 1995). The present results provide a new concept that can relate mechanisms of the excitability control and the volume regulation in CNS neurons, which may lead to the better understanding of epilepsy.

References

Anderson, A.W., Zhong, J., Petroff, O.A., Szafer, A., Ransom, B.R., Prichard, J.W., Gore, J.C., 1996. Effects of osmotically driven cell volume changes on diffusion-weighted imaging of the rat optic nerve. Magn. Reson. Med. 35, 162-7.

Andrew, R.D., Fagan, M., Ballyk, B.A., Rosen, A.S., 1989. Seizure susceptibility and the osmotic state. Brain Res. 498, 175-180.

Andrew, R.D., MacVicar, B.A., 1994. Imaging cell volume changes and neuronal excitation in the hippocampal slice. Neuroscience 62, 371-383.

Andrew, R.D., Adamus, J.R., Polischuk, T.M., 1996. Imaging NMDA- and kainate-induced intrinsic optical signals from the hippocampal slice. J. Neurophysiol. 76, 2707-2717.

Andrew, R.D., Jarvis, C.R., Obeidat, A.S., 1999. Potential sources of intrinsic optical signals imaged in live brain slices. Methods 18, 185-196.

Asada, H., Kawamura, Y., Maruyama, K., Kume, H., Ding, R., Ji, F.Y., Kanbara, N., Kuzume, H., Sanbo, M., Yagi, T., Obata, K., 1996. Mice lacking the 65 kDa isoform of glutamic acid decarboxylase (GAD65) maintain normal levels of GAD67 and GABA in their brains but are susceptible to seizures. Biochem. Biophys. Res. Commun. 229, 891-895.

Ballyk, B.A., Quackenbush, S.J., Andrew, R.D., 1991. Osmotic effects on the CA1 neuronal population in hippocampal slices with special reference to glucose. J. Neurophysiol. 65, 1055-1066.

Basavappa, S., Ellory, J.C., 1996. The role of swelling-induced anion channels during neuronal volume regulation. Mol. Neurobiol. 13, 137-153.

Cossart, R., Dinocourt, C., Hirsch, J.C., Merchan-Petez, A., Felipe, J.D., Ben-Ari, Y., Esclapez, M., Bernard, C., 2001. Dendritic but not somatic GABAergic inhibition is decreased in experimental epilepsy. Nature Neurosci. 4, 52-62.

D'Arcangelo, G., Tancredi, V., Avoli, M., 2001. Intrinsic optical signals and electrographic seizures in the rat limbic system. Neurobiology of Disease 8, 993-1005

Darquie, A., Poline, J.B., Poupon, C., Saint-Jalmes, H., Bihan, D.L., 2001. Transient decrease in water diffusion observed in human occipital cortex during visual stimulation. Proc. Natl. Acad. Sci. USA 98, 9391-9395.

Dietzel, I., Heinemann, U., Hofmeier, G., Lux, H.D., 1980. Transient changes in the size of the extracellular space in the sensorimotor cortex of cats in relation to stimulus-induced changes in potassium concentration. Exp. Brain Res. 40, 432-439.

Dodt, H.U., D'Arcangelo, G., Pestel, E., Zieglgänsberger, W., 1996. The spread of

excitation in neocortical columns visualized with infrared-darkfield videomicroscopy. Neuroreport 7, 1553-1558.

Dudek, F.E., Obenaus, A., Tasker, J.G., 1990. Osmolality-induced changes in extracellular volume alter epileptiform bursts independent of chemical synapses in the rat: importance of non-synaptic mechanisms in hippocampal epileptogenesis. Neurosci. Lett. 120, 267-270.

Dudek, F.E., Yasumura, T., Rash, J.E., 1998. 'Non-synaptic' mechanisms in seizures and epileptogenesis. Cell Biol. Int. 22, 793-805.

During, M.J., Spencer, D.D., 1993. Extracellular hippocampal glutamate and spontaneous seizure in the conscious human brain. The Lancet 341, 1607-10.

Evans, M.G., Marty, A., Tan, Y.P., Trautmann, A., 1986. Blockage of Ca-activated Cl conductance by furosemide in rat lacrimal glands. Pflugers Arch. 406, 65-8.

Frostig, R.D., Lieke, F.E., Ts'o, D.Y., Grinvald, A., 1990. Cortical functional architecture and local coupling between neuronal activity and the microcirculation revealed by in vivo high-resolution optical imaging of intrinsic signals. Proc. Natl. Acad. Sci. USA 87, 6082-6.

Grinvald, A., Lieke, E., Frostig, R.D., Gilbert, C.D., Wiesel, T.N., 1986. Functional architecture of cortex revealed by optical imaging of intrinsic signals. Nature 324, 361-4.

Haglund, M.M., Ojemann, G.A., Hochman, D.W., 1992. Optical imaging of epileptiform and functional activity in human cerebral cortex. Nature 358, 668-671.

Hochman, D.W., Baraban, S.C., Owens, J.W.M., Schwartzkroin, P.A., 1995. Dissociation of synchronization and excitability in furosemide blockage of epileptiform activity. Science 270, 99-102.

Holthoff, K., Witte, O.W., 1996. Intrinsic optical signals in rat neocortical slices measured with near-infrared dark-field microscopy reveal changes in extracellular space. J. Neurosci. 16, 2740-2749.

Holthoff, K., Witte, O.W., 2000. Directed spatial potassium redistribution in rat neocortex. Glia 29, 288-292.

Isokawa, M., 1996. Decrement of $GABA_A$ receptor-mediated inhibitory postsynaptic current in dentate granule cells in epileptic hippocampus. J. Neurophysiol. 75, 1901-8.

Isokawa, M., 2000. Altered pattern of transmittance and resistance to AMPA-induced swelling in the dentate gyrus of the epileptic hippocampus. Hippocampus 10, 663-672.

Isokawa, M., Mathern, G.W., 1999. Developmental changes in NMDA-induced intrinsic optical signals in the hippocampal dentate gyrus of children with medically intractable seizures. Dev. Neurosci. 21, 215-22.

Inglefield, J.R., Schwartz-Bloom, R.D., 1998. Activation of excitatory amino acid receptors in the rat hippocampal slice increases intracellular Cl^- and cell volume. J. Neurochem. 71, 1396-1404.

Jarvis, C.R., Lilge, L., Vipond, G.J., Andrew, R.D., 1999. Interpretation of intrinsic optical signals and calcein fluorescence during acute excitotoxic insult in the hippocampal slice. Neuro Image 10, 357-372.

Jefferys, J.G.R., 1995. Nonsynaptic modulation of neuronal activity in the brain: electric currents and extracellular ions. Physiological Reviews 75, 689-715.

Johnson, L.J., Hanley, D.F., Thakor, N.V., 2000. Optical light scatter imaging of cellular and sub-cellular morphology changes in stressed rat hippocampal slices. J. Neurosci. Methods 98, 21-31.

Kirino, T., 1982. Delayed neuronal death in the gerbil hippocampus following ischemia. Brain Res 239:57-69.

Kohn, A., Metz, C., Quibrera, M., Tommerdahl, M.A., Whitsel, B.L., 2000. Functional neocortical microcircuitry demonstrated with intrinsic signal optical imaging in vitro. Neurosci. 95, 51-62

Kreisman, N.R., LaManna, J.C., Liao, S., Yeh, E.R., Alcala, J.R., 1995. Light

transmittance as an index of cell volume in hippocampal slices: optical differences of interfaced and submerged positions. Brain Res. 693, 179-186.

Lipton, P., 1973. Effects of membrane depolarization on light scattering by cerebral cortical slices. J. Physiol. 231, 365-383.

McBain, C.H., Traynelis, S.F., Dingledine, R., 1990. Regional variation of extracellular space in the hippocampus. Science 249, 674-677.

MacVicar, B.A., Hochman, D., 1991. Imaging of synaptically evoked intrinsic optical signals in hippocampal slices. J. Neurosci.11, 1458-1469.

MacVicar, B.A., Feighan, D., Brown, A., Ransom, B., 2002. Intrinsic optical signals in the rat optic nerve: Role for K^+ uptake via NKCC1 and swelling of astrocytes. Glia 37, 114-123.

Martin, L.A., Wei, D.S., Alger, B.E., 2001. Heterogeneous susceptibility of $GABA_A$ receptor-mediated IPSCs to depolarization-induced suppression of inhibition in rat hippocampus. J. Physiol. 532, 685-700.

Momose-Sato, Y., Sato, K., Hirota, A., Kamino, K., 1998. GABA-induced intrinsic light-scattering changes associated with voltage-sensitive dye signals in embryonic brain stem slices: Coupling of depolarization and cell shrinkage. J. Neurophysiol. 79, 2208-17.

Morin, F., Beaulieu, C., Lacaille, J., 1999. Alterations of perisomatic GABA synapses on hippocampal CA1 inhibitory interneurons and pyramidal cells in the kainate model of epilepsy. Neuroscience 93, 457-467.

Morishima, S., Shimizu, T., Kida, H., Okada, Y., 2000. Volume expansion sensitivity of swelling-activated Cl^- channel in human epithelial cells. Japanese J. Physiol. 50, 277-280

Murase, K., Saka,T., Terao, S., Ikeda, H., Asai, T., 1998. Slow intrinsic optical signals in the rat spinal dorsal horn in slice. Neuroreport 9, 3663-3667.

Nicholson, C., 1992. Quantitative analysis of extracellular space using the method of TMA^+ iontophoresis and the issue of TMA^+ uptake. Can. J. Physiol. Pharmac. 70, S314-S322.

Nicholson, C., Sykova, E., 1998. Extracellular space structure revealed by diffusion analysis. Trends Neurosci. 21, 207-215.

Okada, Y., Maeno, E., Shimizu, T., Dezaki, K., Wang, J., Morishima, S., 2001. Receptor-mediated control of regulatory volume decrease (RVD) and apoptotic volume decrease (AVD). J. Physiol. 532, 3-16.

Paulsen, R.E., Contestabile, A, Villani, L., Fonnum, F., 1987. An in vivo model for studying function of brain tissue temporarily devoid of glial cell metabolism: the use of fluorocitrare. J. Neurochem. 48, 1377-1385.

Pearce, R.A., 1993. Physiological evidence for two distinct GABAA responses in rat hippocampus. Neuron 10, 189-200.

Prichard, J.W., Zhong, J., Petroff, O.A., Gore, J.C., 1995. Diffusion-weighted NMR imaging changes caused by electrical activation of the brain. NMR Biomed. 8 (7-8), 359-64.

Pulsinelli, W.A., Brierley, J.B., Plum, F., 1982. Temporal profile of neuronal damage in a model of transient forebrain ischemia. Ann Neurol 11, 491-8.

Rosen, A.S., Andrew, R.D., 1990. Osmotic effects upon excitability in rat neocortical slices. Neurosci. 38, 579-590.

Schwartzkroin, P.A., Baraban, S.C., Hochman, D.W., 1998. Osmolarity, ionic flux, and changes in brain excitability. Epilepsy Res. 32, 275-285.

Shoham, D., Grinvald, A., 2001. The cortical representation of the hand in macaque and human area S-I: high resolution optical imaging. J. Neurosci. 21, 6820-35.

Strange, K., Emma, F., Jackson P.S., 1996. Cellular and molecular physiology of volume-sensitive anion channels. Am. J. Physiol. 270, C711-C730.

Tian, N., Peterson, C., Kash, S., Baekkeskov, S., Copenhagen, D., Nicoll, R., 1999. The

role of the synthetic enzyme GAD65 in the control of neuronal γ-aminobutyric acid release. Proc. Natl. Acad. Sci. USA 96, 12911-12916.

Trachsel, L., Dodt, H.U., Zieglgänsberger,W., 1996. The intrinsic optical signal evoked by chiasm stimulation in the rat suprachiasmatic nuclei exhibits GABAergic day-night variation. Eur. J. Neurosci. 8, 319-328.

Traynelis, S.F., Dingledine, R., 1989. Role of extracellular space in hyperosmotic suppression of potassium-induced electrographic seizures. J. Neurophysiol. 61, 927-938.

Turner, D.A., Aitken, P.G., Somjen G.G., 1995. Optical mapping of translucence changes in rat hippocampal slices during hypoxia. Neurosci. Lett. 195, 209-213.

Witte, O.W., Niermann, H., Holthoff, K., 2001. Cell swelling and ion redistribution assessed with intrinsic optical signals. An. Acad. Bras. Cienc. 73, 337-350.

Yoshioka, K., Nisimaru, N., Yanai, S., Shimoda, H., Yamada, K., 2000. Characteristics of monocarboxylates as energy substrates other than glucose in rat brain slices and the effect of selective glial poisoning- a ^{31}P NMR study. Neurosci. Res. 36, 215-226

Zhong, J., Petroff, O.A., Pleban, L.A., Gore, J.C., Prichard, J.W., 1997. Reversible, reproducible reduction of brain water apparent diffusion coefficient by cortical electroshocks. Magn. Reson. Med. 37 (1), 1-6.

Acknowledgements

I would like to express my sincere appreciation to Dr. Hiroshi Tsubokawa (National Institute for Physiological Sciences) for his generous support and valuable guidance throughout this research. I am also sincerely grateful to Dr. Kunihiko Obata (National Institute for Physiological Sciences) for helpful supports of GAD65 KO mice, Dr. Shin-ichiro Mori (National Institute for Physiological Sciences) for cooperation throughout two-photon experiments.

Figure Legends

Figure 1. Schematic drawing of the experimental setup.

The slices were trans-illuminated by near-infrared light (775 ± 15 nm) through band path filter (IR filter). Images of near-infrared light (IR) transmittance were obtained by using a cooled CCD camera system. Extracellular field potentials were recorded simultaneously from stratum radiatum of the CA1 region.

Figure 2. Relationship between changes in light transmittance and bath osmolality.

A: Time dependent changes in light transmittance during hypotonic conditions. Transmittance was imaged from a slice placed on the recording chamber, and perfusing solution was replaced with hypo-osmotic solution (324, 314, 304 mOsm) during 300-1200 sec (dotted lines). The blue line indicates average signals obtained from rectangular region shown the IR image (right picture, P; stratum pyramidale, R; stratum radiatum). Osmolarities of test solutions were indicated on each trace. **B:** Changes in light transmittance as a function of bath osmolarity. Straight line has been made by linear regression. Square region by broken line indicates a range of the data in A. Vertical bars represent ± SD of the mean (n = 6). **C:** Speculative relationship between changes in light transmittance and relative cell volume (V/V_0) (See details in text).

Figure 3. Transient increases in IR transmittance in the hippocampal CA1 region induced by repeated synaptic input.

A: Basic arrangement for the experiment. The lower picture is a sample image of near-infrared (775 ± 15 nm) light transmittance. O, stratum oriens; P, stratum pyramidale;

R, stratum radiatum. Blue (dendritic region) and red (somatic region) rectangular regions indicate areas for signal measurement. **B:** Typical records of extracellular field potential (upper trace) and changes in IR transmittance (lower graph). Traces were obtained from a single trial. The dotted line and the arrow designated 'HFS' indicate time of high frequency stimulation. Blue and red lines indicate signals obtained from dendritic and somatic regions, shown in panel A, respectively. A high magnification of the trace of field potential is shown in the inset.

Figure 4. Morphological changes of a CA1 pyramidal neuron in the hippocampal slice after synaptic input.

A: Left: Time course of changes in light transmittance and the sampling periods (color bar ①control (blue), ②after stimulation (orange), ③recovery (purple)). Blue and red lines represent time dependent changes in light transmittance obtained from dendritic and somatic regions, respectively. Repetitive stimulation was delivered during time 0-30 sec shown as a pair of dotted lines. Right: Pictures of a stained pyramidal neuron at each sampling period (①control, ②after stimulation, ③recovery) corresponded to the period shown by color bar in the left graph. Bar = 10 μm. **B:** Morphological changes of the pyramidal neuron (same as a neuron shown in A). Cross-sectional area of midline section of somato-dendritic axis in each period of cell were measured and plotted against distances from head of the soma. Blue, orange and purple bars indicate periods of control, after stimulation and recovery, respectively. Definitions for the measurement were shown in the inset. **C:** Normalized changes in section areas during event. Data were obtained from 6 neurons. Distance as a landmark (distance 0) was adjusted at a section showing maximum section area. Orange triangle indicates the data from 'after stimulation', and

purple filled circle indicate the data from 'recovery'. Vertical bars represent ± SD of the mean. Asterisks on each bar indicate significant differences between 'after stimulation' and 'recovery' (Student T-test, $P < 0.01$).

Figure 5. Properties of the IR transmittance as a function of stimulus parameters. **A:** Peak amplitude of the signals plotted against the stimulus frequency. Number of pulses was 20, and stimulus intensity was 20 μA (n = 4). **B:** Peak amplitude of the signals plotted against the number of pulses. Frequency was 100 pulses/sec, and intensity was 20 μA (n = 3). **C:** Peak amplitude of the signals plotted against the stimulus intensity. Frequency was 100 pulses/sec, and number of pulses was 20 (n = 3). Example traces of field potentials recorded from the somatic region at 20 μA and at 80 μA are shown in the inset. Blue and red lines indicate data obtained from dendritic (Rad) and somatic (Pyr) regions. Vertical bars represent ± SD of the mean.

Figure 6. Effects of glutamate receptor antagonists. **A:** Effects of bath applied APV (50 μM) and CNQX (10 μM) on field EPSPs. Upward arrows indicate artifacts of stimulation. Each record is an average trace of 8 consecutive trials. **B:** Representative effects of drug application (50 μM APV and 10 μM CNQX) on stimulus-induced changes in IR transmittance. Dotted lines indicate the time of tetanic stimulation. Blue and red lines represent the signals obtained from dendritic and somatic regions, respectively. Traces were obtained from a single trial under each condition. **C:** Summarized data obtained from control 40 slices and from 9 slices in the presence of APV and CNQX. The ordinate indicates peak amplitude of the signals. Blue bars indicate mean ± SD for dendritic regions (Rad), and red bars data for somatic regions (Pyr). Peak

amplitude of the signals in the presence of the drugs was significantly smaller than in the controls (Student T-test, $P < 0.01$).

Figure 7. Effects of a GABA-A receptor antagonist.

A: Effects of bath applied bicuculline (20 μM) on field EPSPs. Upward pointing arrows indicate artifacts of stimulation. Each record is an average trace of 8 consecutive trials. Sample traces (**B**) and summarized data (**C**) are illustrated. Data in C were obtained from 40 control slices and 17 slices in the presence of bicuculline. Peak amplitude of the signals in the presence of drugs was significantly smaller than in controls (Student T-test, $P < 0.01$).

Figure 8. Effects of reducing the Cl^- concentration on optical signals.

A: Stimulus-induced changes in IR transmittance. Extracellular concentrations of Cl^- are indicated on the top of each graph. **B:** Effects of bath applied bicuculline (20 μM) with low-Cl^- solution on optical signals. Dotted lines indicate the time of tetanic stimulation.

Figure 9. Stimulus-induced change in IR transmittance is reduced in GAD65(−/−) mice.

A: Typical traces for field EPSPs. Upward pointing arrows indicate artifacts of stimulation. Each record is the average trace of 8 consecutive trials. **B:** Representative effects of stimulus induced changes on IR transmittance obtained from a wild-type mouse (Wild-type) and from a GAD65(−/−) mutant mouse (GAD65(−/−)). **C:** Summarized data obtained from 10 wild-type slices as controls and from 14 slices from mutant mice. Data are illustrated as in Fig. 3C and 4C. Peak amplitude of the signals obtained from mutant mice was significantly smaller than that from wild-type mice (Student T-test, $P < 0.01$).

Note the lack of effects of bicuculline on optical signals in GAD65(−/−) mice.

Figure 10. Hypothesized model of activity-dependent swelling in the hippocampal CA1 neuron.

When GABAergic inhibitory input is temporally coincident with glutamatergic excitatory input (①), Na^+ and Ca^{2+} influxes through glutamate receptors and Cl^- influx through GABA-A receptor (②) induce an increase in intracellular osmotic pressure, which is resulted in facilitation of water influx into the cell (③).

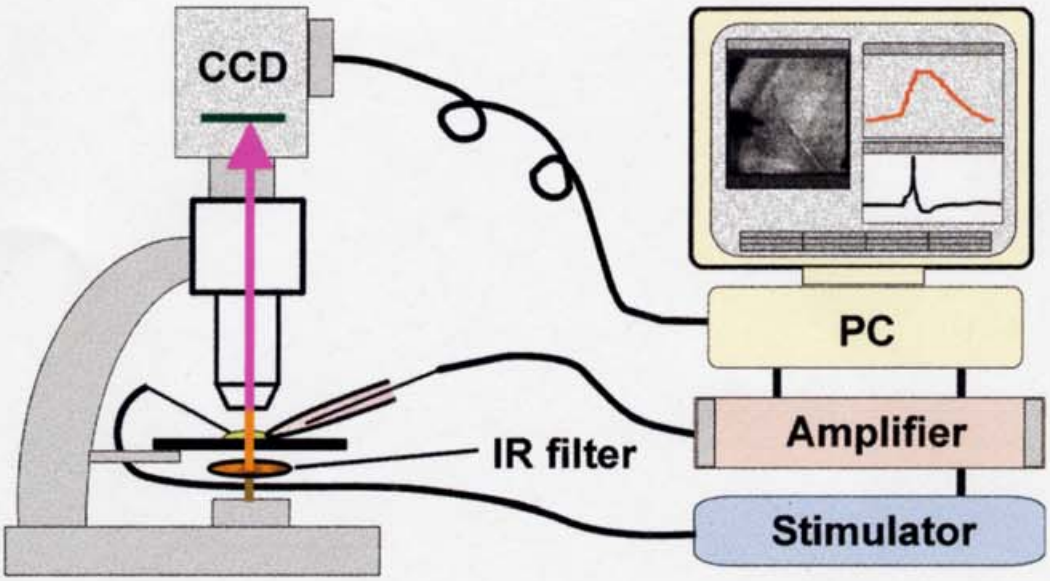

Figure 1.

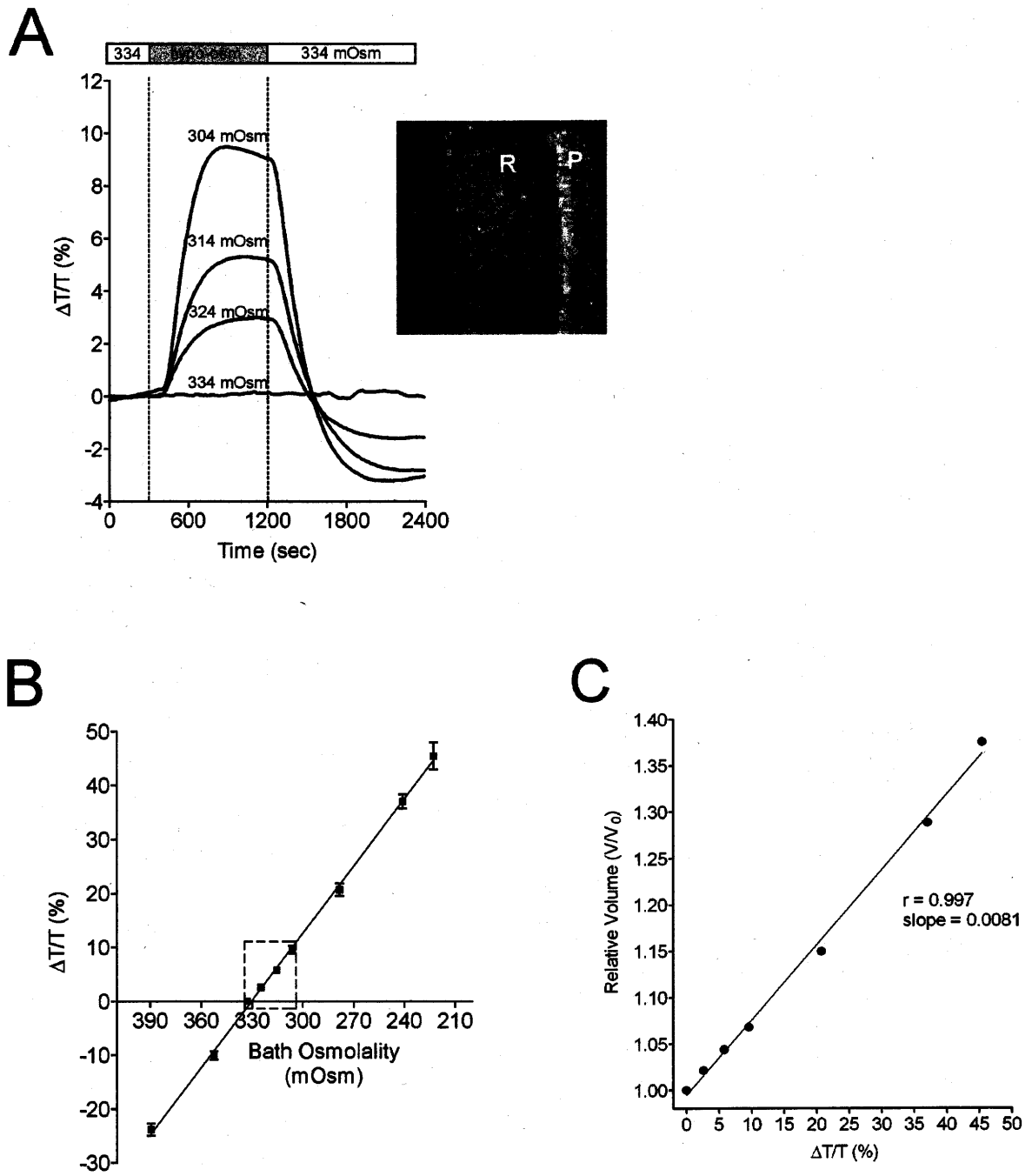
A
334
334 mOsm
304 mOsm
314 mOsm
324 mOsm
334 mOsm
ΔT/T (%)
Time (sec)
R
P
B
ΔT/T (%)
Bath Osmolality (mOsm)
C
Relative Volume (V/V0)
ΔT/T (%)
r = 0.997
slope = 0.0081

Figure 2.

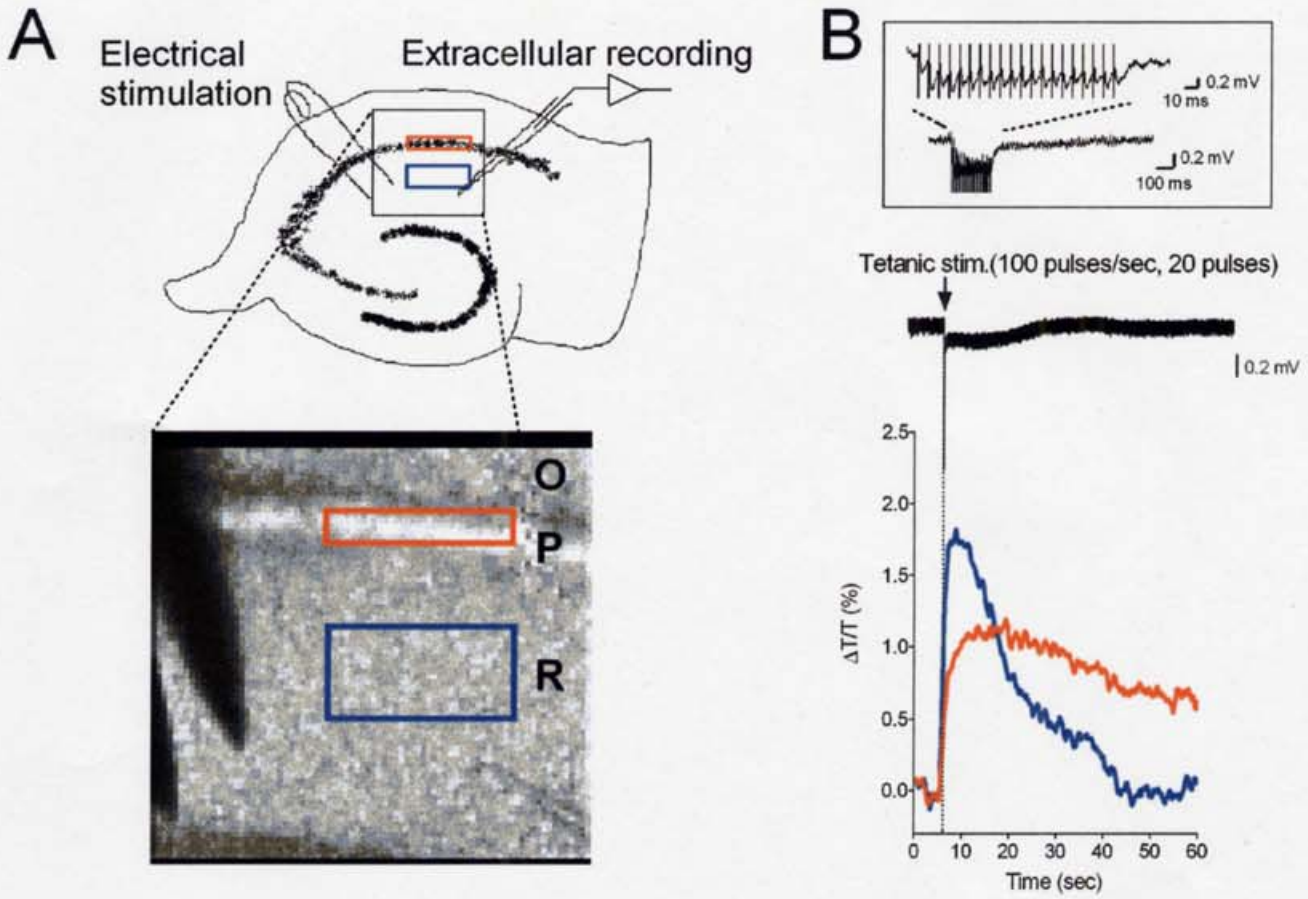
A
Electrical stimulation
Extracellular recording
O
P
R
B
0.2 mV
10 ms
0.2 mV
100 ms
Tetanic stim.(100 pulses/sec, 20 pulses)
0.2 mV
ΔT/T (%)
2.5
2.0
1.5
1.0
0.5
0.0
0
10
20
30
40
50
60
Time (sec)

Figure 3.

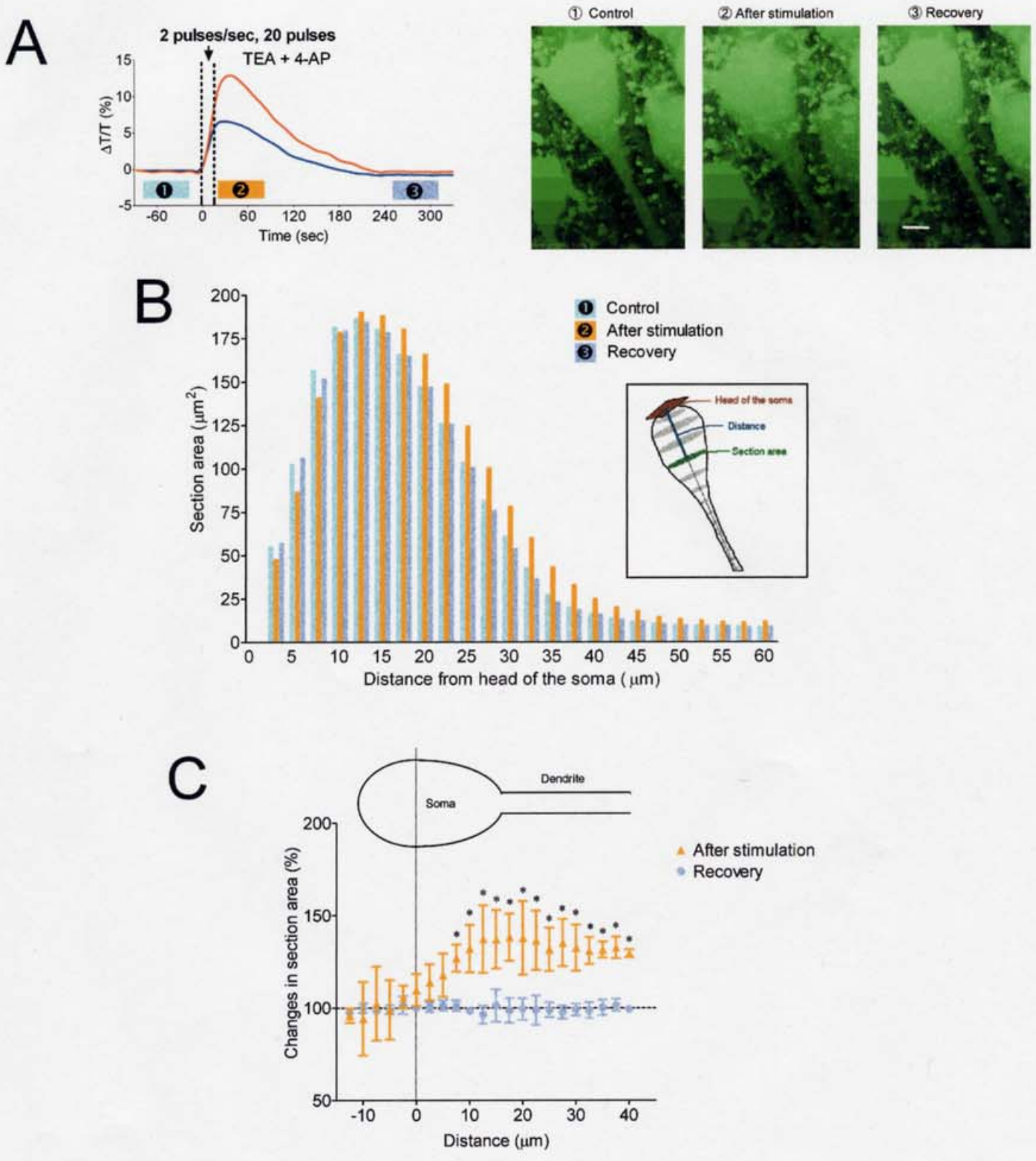
A
2 pulses/sec, 20 pulses
TEA + 4-AP
ΔT/T (%)
Time (sec)
① Control
② After stimulation
③ Recovery
B
Control
After stimulation
Recovery
Head of the soma
Distance
Section area
Section area (μm²)
Distance from head of the soma (μm)
C
Dendrite
Soma
After stimulation
Recovery
Changes in section area (%)
Distance (μm)

Figure 4.

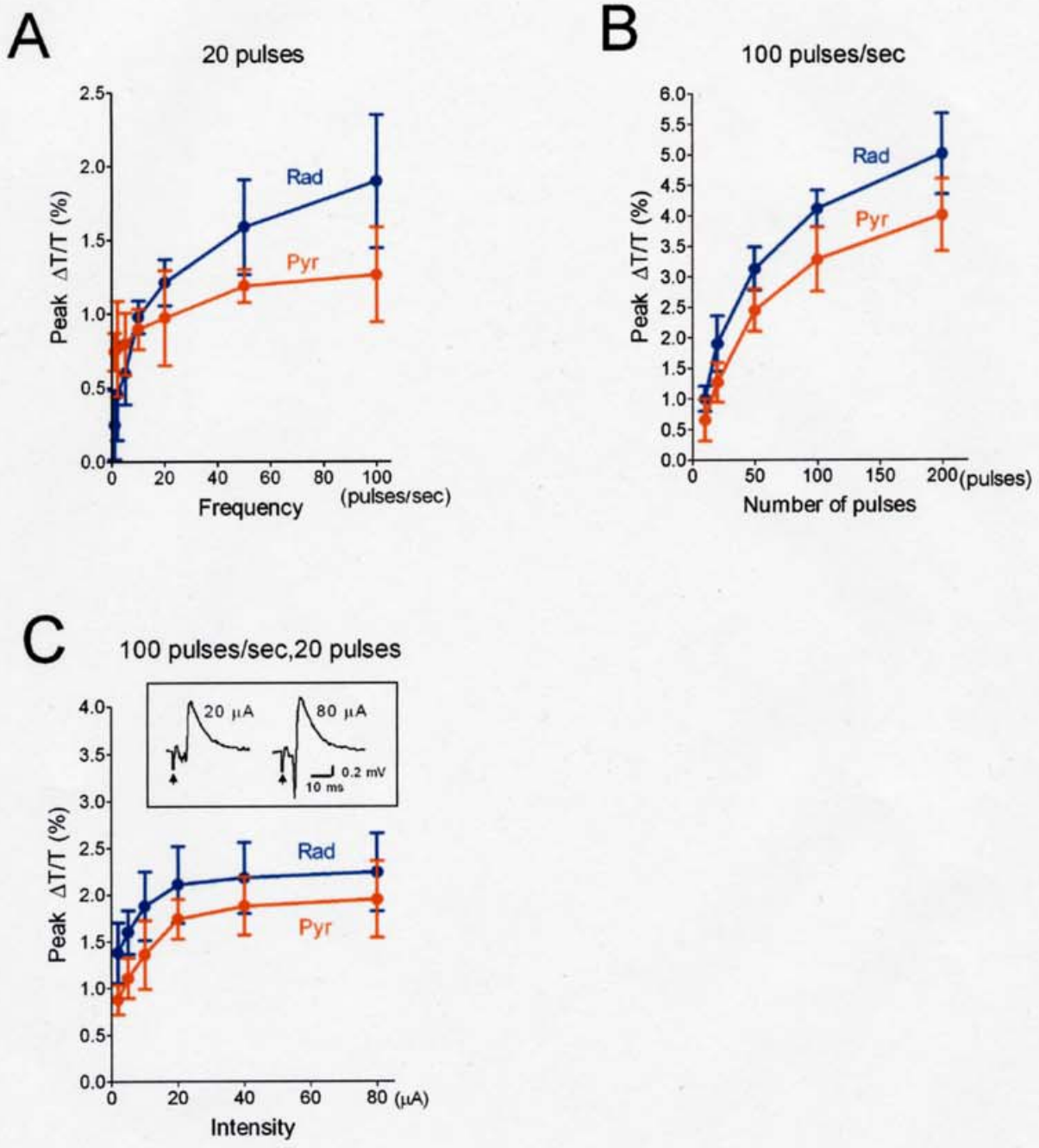
A
20 pulses
Peak ΔT/T (%)
Rad
Pyr
Frequency
(pulses/sec)
B
100 pulses/sec
Peak ΔT/T (%)
Rad
Pyr
Number of pulses
(pulses)
C
100 pulses/sec,20 pulses
20 μA
80 μA
0.2 mV
10 ms
Peak ΔT/T (%)
Rad
Pyr
Intensity
(μA)

Figure 5.

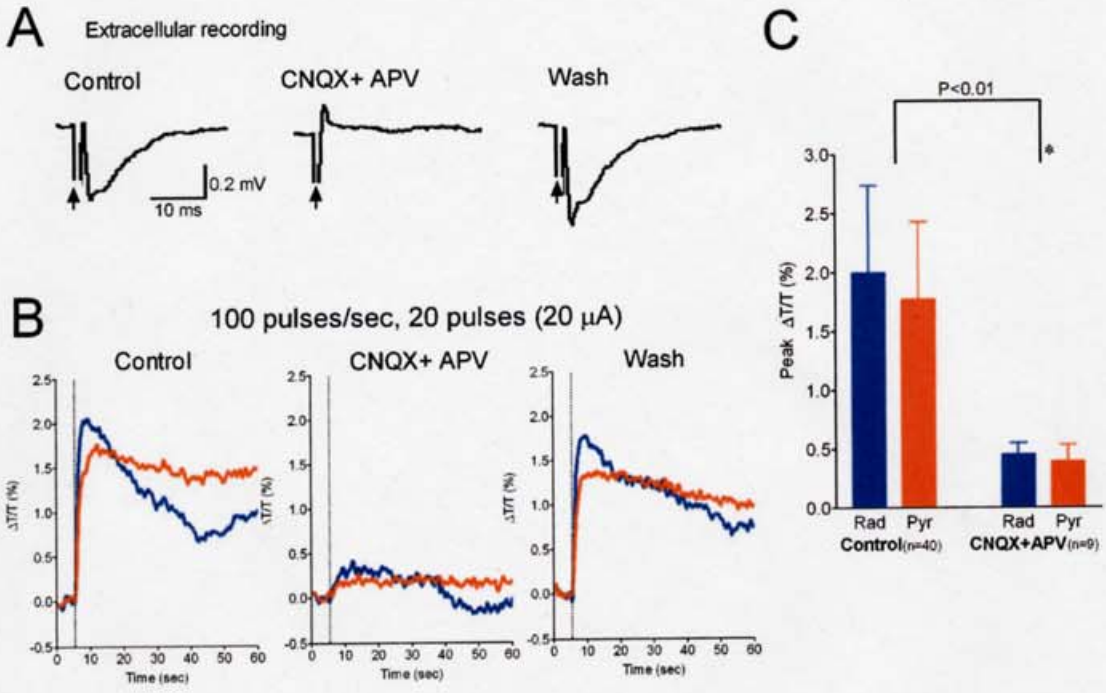
A
Extracellular recording
Control
CNQX+ APV
Wash
0.2 mV
10 ms
B
100 pulses/sec, 20 pulses (20 μA)
Control
CNQX+ APV
Wash
ΔT/T (%)
Time (sec)
C
P<0.01
Peak ΔT/T (%)
Rad
Pyr
Control(n=40)
CNQX+APV(n=9)

Figure 6.

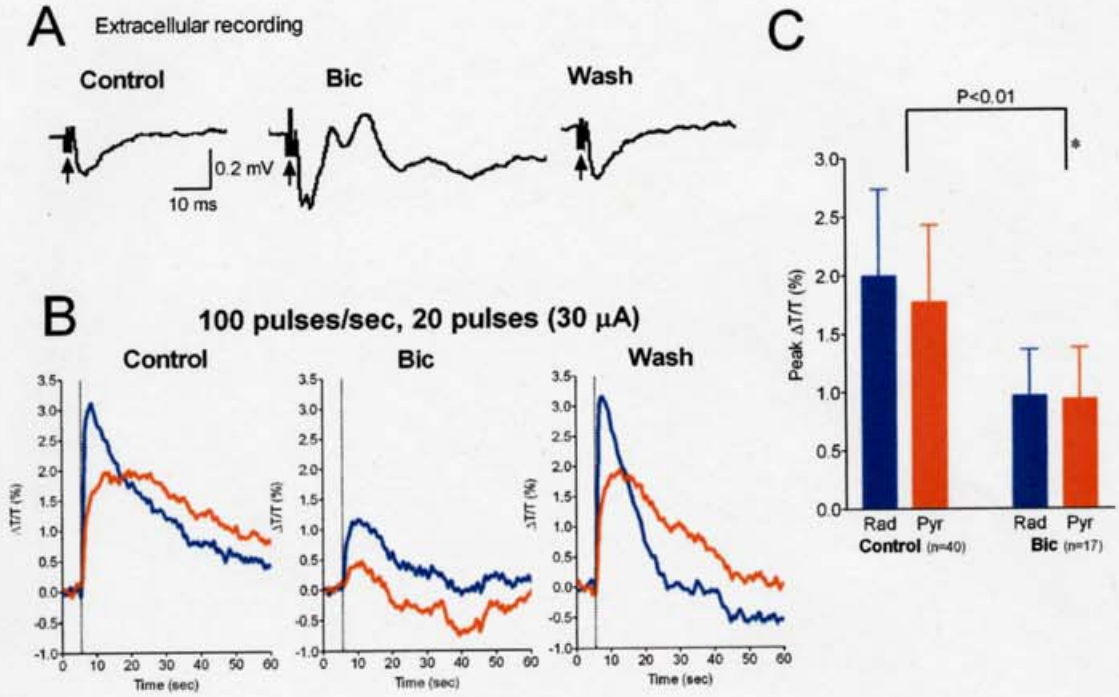
A
Extracellular recording
Control
Bic
Wash
0.2 mV
10 ms
B
100 pulses/sec, 20 pulses (30 μA)
Control
Bic
Wash
ΔT/T (%)
Time (sec)
C
P<0.01
*
Peak ΔT/T (%)
Rad
Pyr
Control (n=40)
Rad
Pyr
Bic (n=17)

Figure 7.

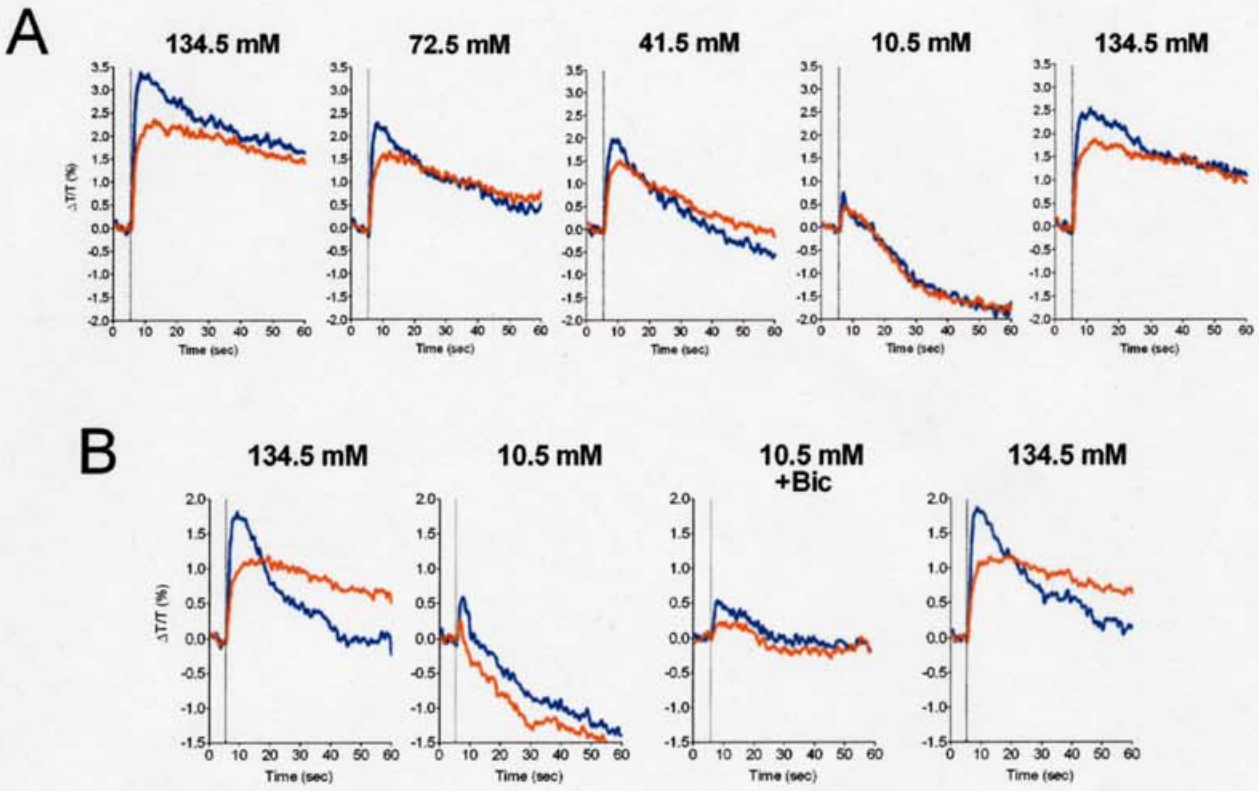
A
134.5 mM
72.5 mM
41.5 mM
10.5 mM
134.5 mM
ΔT/T (%)
Time (sec)
B
134.5 mM
10.5 mM
10.5 mM
+Bic
134.5 mM
ΔT/T (%)
Time (sec)

Figure 8.

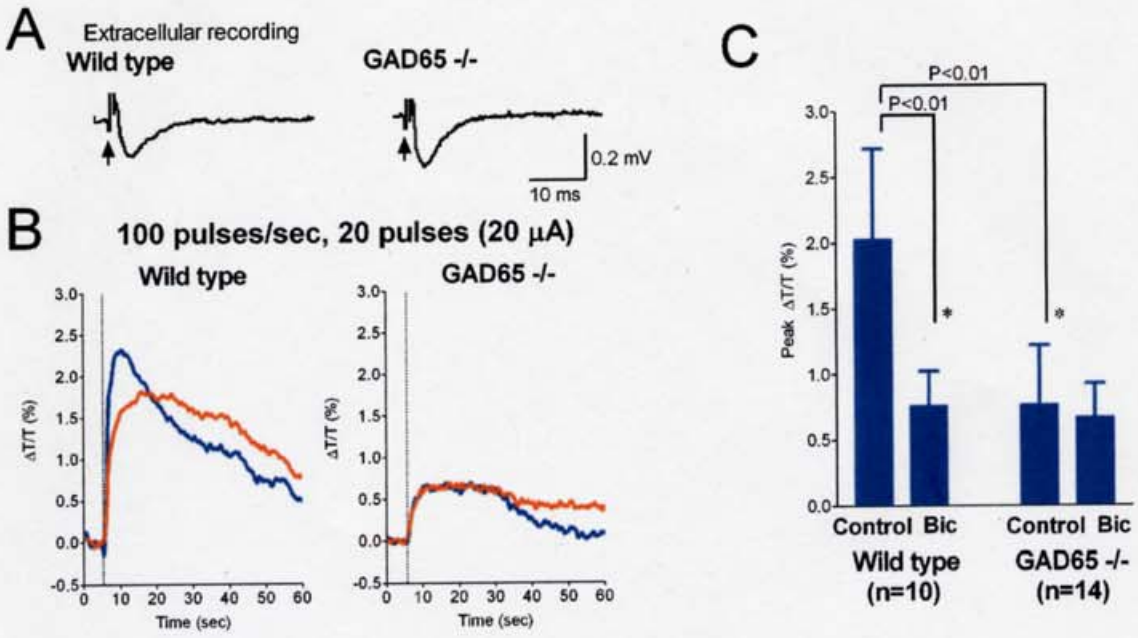
A
Extracellular recording
Wild type
GAD65 -/-
0.2 mV
10 ms
B
100 pulses/sec, 20 pulses (20 μA)
Wild type
GAD65 -/-
ΔT/T (%)
Time (sec)
C
P<0.01
P<0.01
Peak ΔT/T (%)
Control Bic
Control Bic
Wild type
(n=10)
GAD65 -/-
(n=14)

Figure 9.

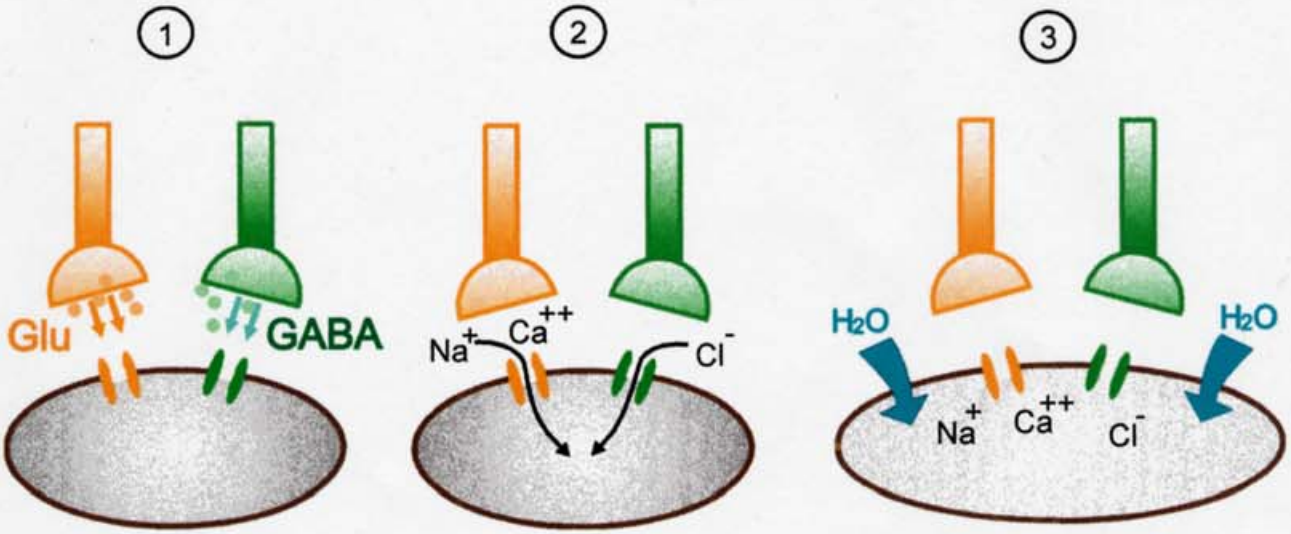

Figure 10.

Table 1. Contribution of other Cl^- pathways.

Inhibitor	Conc.	Effect on peak signal	Possible targets	Amplitude of field potential	n
Bumetanide	100 μM	NC	$Na^+/K^+/2Cl^-$ co-transporter	NC	6
Furosemide	100 μM	NC	$Na^+/K^+/2Cl^-$ co-transporter	NC	6
			K^+/Cl^- co-transporter		
	2.5 mM	Decrease	GABA-A receptor	Increase	6
		(48± 7%)	Ca^{2+}-activated Cl^- channel	(164± 11%)	
DIDS	20 μM	NC	HCO_3^-/Cl^- exchanger	NC	5
			Ca^{2+}-activated Cl^- channel		
NPPB	100 μM	NC	Voltage-dependent Cl^- channel	NC	4
			Volume-sensitive Cl^- channel		
IAA-94	100 μM	NC	Voltage-dependent Cl^- channel	NC	5
Glibenclamide	100 μM	NC	CFTR·Cl^- channel	NC	4

DIDS, 4,4'-diisothiocyanatostilbene-2,2'-disulfonic acid; NPPB, 5-nitro-2-(3-phenylpropylamino-benzoate); IAA-94, r-[+]-methylindazone

NC, No significant change (Student T-test, $P > 0.05$).